

# Pressure and Temperature Transformations of the Molecular Conformation and Crystal Structure of Ferrocene $\text{Fe}^{2+}(\eta^5\text{-C}_5\text{H}_5)_2^-$

Alexey V. Kuzmin,\* Konstantin P. Meletov, and Maxim A. Faraonov

Cite This: *J. Phys. Chem. C* 2022, 126, 3688–3695

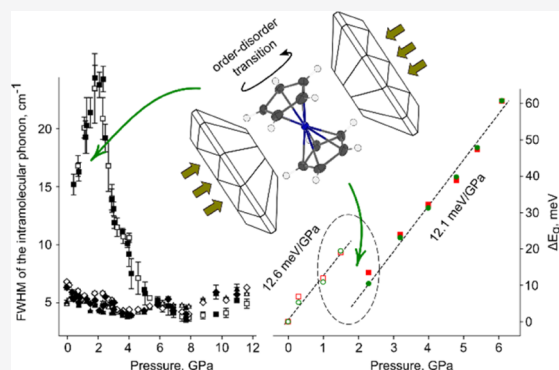
Read Online

ACCESS |

Metrics & More

Article Recommendations

**ABSTRACT:** X-ray diffraction, optical spectroscopy, and numerical calculations were carried out on pristine ferrocene  $\text{Fe}^{2+}(\eta^5\text{-C}_5\text{H}_5)_2^-$  single crystals under various pressure/temperature conditions. Structural data were obtained at room temperature and pressures up to 6.5 GPa as well as at ambient pressure and low temperatures up to 100 K. The iron–carbon bond length ( $l = 2.043 \text{ \AA}$  under ambient conditions) shows linear temperature dependence and quadratic pressure dependence with the coefficients  $\partial l/\partial T = -2.84 \times 10^{-5} \text{ \AA K}^{-1}$ ,  $\partial l/\partial P = -1.36 \times 10^{-3} \text{ \AA GPa}^{-1}$ , and  $\partial^2 l/\partial P^2 = -3.04 \times 10^{-4} \text{ \AA GPa}^{-2}$ , respectively. Jumping of the Fc molecular configuration between  $D_{5h}$  and  $D_{5d}$  conformations decreases at high pressure/low temperature, leading to complete ordering in low-temperature (LT, <161.3 K) and high-pressure (HP, >3 GPa) phases. The initially large bandwidth of lattice phonon modes increases with pressure to a maximum at 2 GPa and decreases to the common value after molecular ordering at pressures  $P > 3 \text{ GPa}$ . The electronic structure calculations in the HP phase at high pressure show a linear increase in the fundamental gap  $E_g$  with the pressure coefficient of 28 meV/GPa. Optical transmission measurements at high pressure demonstrate an almost 2 times smaller pressure coefficient of about 12 meV/GPa and an abrupt decrease in the gap by  $\sim 14.5 \text{ meV}$  at  $P = 2 \text{ GPa}$ .



## 1. INTRODUCTION

Bis(cyclopentadienyl)iron  $\text{Fe}^{2+}(\eta^5\text{-C}_5\text{H}_5)_2^-$  or ferrocene (Fc) is a well-known example of a sandwich-type organometallic molecule, which has been effectively studied since its discovery in 1951.<sup>1,2</sup> Cyclopentadienyl (Cp), a  $\pi$ -conjugated  $\text{C}_5\text{H}_5$  ring in a Fc molecule, is extremely mobile and has a tendency for jumping rotations around the  $\text{C}_5$  molecular axis. Locking positions of Cp correspond to  $D_{5h}$  (eclipsed) and  $D_{5d}$  (staggered) configurations of a Fc molecule. These configurations are very close in energy, while a small energy barrier of about 4.3–66.3 meV/molecule separates them<sup>3–5</sup> so that the eclipsed configuration has smaller energy and is more stable and preferable. For this reason, a free gas-phase Fc molecule tends to take the  $D_{5h}$  configuration, whereas in the solid state, both configurations are present due to the influence of a crystal field.

There are three structural states of Fc crystals: monoclinic phase at atmospheric pressure/room temperature—APRT; low-temperature triclinic phase— $\text{LT}_1$ ; low-temperature orthorhombic phase— $\text{LT}_2$ ; and high-pressure monoclinic phase—HP. Under ambient conditions, Fc crystallizes into the monoclinic APRT phase with dynamically disordered  $\text{C}_5\text{H}_5$  rings. The common triclinic  $\text{LT}_1$  phase was fully described by Seiler and Dunitz.<sup>6</sup> According to calorimetry data, the transition between the APRT and  $\text{LT}_1$  phases occurs near 163.9 K.<sup>7</sup> Ogasahara et al. revealed the metastable nature of the

$\text{LT}_1$  phase,<sup>8</sup> assuming the APRT phase as undercooled at this temperature. The slow heating of the  $\text{LT}_1$  phase obtained in this way followed by annealing at 190 K led to its stabilization and subsequent  $\text{LT}_1 \rightarrow \text{APRT}$  transition at a temperature of about 246 K. The orthorhombic low-temperature  $\text{LT}_2$  phase was found by Seiler's group as a result of *in situ* crystallization of Fc crystals from a propanol solution below 110 K.<sup>9</sup> The slow warming of the  $\text{LT}_2$  phase involves the  $\text{LT}_2 \rightarrow \text{APRT}$  transition at 275 K, which suggests also the metastability of the  $\text{LT}_1$  phase with respect to  $\text{LT}_2$ .<sup>9</sup> Based on the structural data, the key difference between two low-temperature phases is related to the mutual orientation of the Fc Cp rings. In the  $\text{LT}_2$  phase, the molecules strongly maintain an eclipsed conformation,<sup>9</sup> while in the  $\text{LT}_1$  phase, the Cp rings of the molecule are turned relative to each other by  $9^\circ$ .<sup>6</sup>

High-pressure phase transition assumptions in Fc crystals were claimed in early publications of Duecker<sup>10</sup> and Zhorin<sup>11</sup> based on their optical and conductivity measurements data at

Received: November 24, 2021

Revised: January 26, 2022

Published: February 9, 2022



high pressure. Later, a highly qualified study of ferrocene crystals at high pressure was carried out by Paliwoda and coauthors, and the new ordered HP phase was described in detail.<sup>12</sup> They claimed an isostructural transition at a critical pressure of 3.24 GPa when the crystal field becomes strong enough and forces Fc molecules to take a staggered configuration.<sup>3,12,13</sup>

In the present study, we have carried out accurate X-ray diffraction, Raman scattering, and optical transmission measurements at high pressure, as well as numerical calculations of the electronic structure of  $\text{Fe}^{2+}(\eta^5\text{-C}_5\text{H}_5)_2$  single crystals. Interest in this investigation was caused by the unusual behavior of a ferrocene molecule that demonstrates gradual axial elongation of the iron-Cp pyramids at high pressure in the molecular donor–acceptor complexes of fullerene.<sup>14,15</sup> We found that the Fe–C bond length ( $l = 2.043 \text{ \AA}$  under ambient conditions) demonstrates linear temperature dependence with the coefficients  $\partial l/\partial T = -2.84 \times 10^{-5} \text{ \AA K}^{-1}$  and quadratic pressure dependence with  $\partial l/\partial P = -1.36 \times 10^{-3} \text{ \AA GPa}^{-1}$  and  $\partial^2 l/\partial P^2 = -3.04 \times 10^{-4} \text{ \AA GPa}^{-2}$ . The intramolecular disordering parameter, associated with two possible occupations of Cp rings and the angle between them, varies with temperature and pressure so that ferrocene molecules become completely ordered in low-temperature ( $<161.3 \text{ K}$ ) and high-pressure ( $>3 \text{ GPa}$ ) phases. The intermolecular phonon modes were assigned by the comparison of the Raman spectra of a ferrocene crystal with the calculated intramolecular phonon modes of a ferrocene molecule. The bandwidth of a single intermolecular phonon band in the Raman spectra increases with pressure, reaching the maximum at 2 GPa with a subsequent gradual decrease to the values compatible with those of intramolecular phonons after molecule ordering in the HP phase. The broad band tends to split at  $P > 3 \text{ GPa}$ , forming five rather sharp peaks at a pressure of 4 GPa after the transition to the HP phase. The numerical calculations of the electronic band structure in the HP phase show a linear increase with pressure of the direct energy gap in the center of the Brillouin zone. The calculated pressure coefficient of 28 meV/GPa differs from that of  $\sim 12 \text{ meV/GPa}$  obtained in the optical transmission measurements at high pressure, which show additionally an abrupt decrease in the fundamental gap by  $\sim 14.5 \text{ meV}$  near 2 GPa.

## 2. EXPERIMENTAL SECTION

Single crystals of pristine ferrocene were obtained by the slow evaporation solvent technique. An orange-colored saturated hexane solution of ferrocene was slowly evaporated, and after being left standing for 1 month at room temperature, small orange Fc rhomboids (about  $0.35 \times 0.35 \times 0.2 \text{ mm}$  in size) were crystallized. The samples obtained in this way were washed in hexane, dried, and stored in a freezer before an X-ray diffraction experiment. The crystals for an X-ray diffraction analysis were carefully selected based on their habitus and faceting. Low-temperature X-ray diffraction experiments were carried out using a Rigaku Oxford Diffraction Gemini R diffractometer with  $\omega$ -scan rotation. Mo  $K_\alpha$  radiation  $\lambda = 0.7107 \text{ \AA}$  and a graphite monochromator were used. The temperature control was performed using an Oxford CryoJet cooling system within the range of 100–300 K. To minimize sublimation, single crystals of Fc were first cooled down to 100 K and then heated slowly with the simultaneous diffraction data recording. An effective heating rate of  $\sim 0.14 \text{ K/min}$  was calculated considering the heating regime, which includes a

two-step increase of temperature by 5 K for 10 min and 1 h of exposure time after every 10 K. High-pressure X-ray diffraction experiments with pressures up to 6.5 GPa were performed *in situ* on the same laboratory diffractometer using a Boehler–Almax design diamond anvil cell (DAC) with a  $42^\circ$  available aperture specially designed for X-ray diffraction studies. The samples were initially placed in a hole  $\sim 200 \mu\text{m}$  in diameter made in a stainless-steel gasket. Silicone oil was used as a pressure-transmitting medium, and a ruby chip fluorescence  $R_1$  line was used for pressure calibration. Structural solution and refinement were performed using *CRYSTALISPRO*,<sup>16</sup> *OLEX2*,<sup>17</sup> and *SHELX*<sup>18</sup> bundles. The structures were solved using direct methods (*SHELXT*<sup>19</sup>). Hydrogen atoms are calculated at idealized positions using the riding model. The refinement of all non-hydrogen atoms was performed in the anisotropic approximation using the *SHELXL* program. During the refinement, all Fe–C and C–C bonds were forced to be the same; moreover, carbon atoms in a separate Cp ring were restricted to move only in the plane of the ring.

The Raman spectra at high pressure were recorded in the back-scattering geometry using a Mao–Bell type DAC and an Acton SpectraPro-2500i spectrograph equipped with a Peltier cooled charge-coupled device and an Olympus microscope for micro-Raman measurements. The optical transmission was measured through the use of downlight illumination of a microscope. Transmitted light was collected from a carefully fixed site of the sample by focusing  $\times 50$  Olympus objective in a  $\sim 1 \mu\text{m}$  spot. The 532 nm line of a single-mode diode-pumped laser was used for Raman scattering measurements. The laser line was suppressed by an edge filter, while the beam intensity before the DAC was about 0.3 mW. The position of phonon bands and their bandwidth in the Raman spectra was defined by fitting of experimental data using the pseudo-Voigt function. The samples  $\sim 100 \mu\text{m}$  in diameter were placed in a hole  $\sim 150 \mu\text{m}$  in diameter made in a stainless-steel gasket predeformed to a thickness of  $\sim 90 \mu\text{m}$ . The methanol–ethanol 4:1 mixture and the ruby fluorescence technique were used as a pressure-transmitting medium and a pressure calibration tool, respectively.

The band structure was calculated by the density functional theory-based tight-binding method using the DFTB+ software<sup>20</sup> with the parameterization sets mio-1-1<sup>21</sup> and trans3d-0-1.<sup>22</sup> The Raman spectra of a Fc molecule were calculated within the density functional theory using the UHF/B3LYP (Becke's three-parameter exchange functional<sup>23</sup> and the Lee–Yang–Parr correlation functional<sup>24</sup>) hybrid method and cc-pVTZ (for light C, H atoms) in combination with the LANL2DZ (for Fe) mixed basis sets implemented in the *FIREFLY* program.<sup>25</sup>

## 3. RESULTS AND DISCUSSION

**3.1. General Structure Description.** The ferrocene single crystals were grown in their stable monoclinic APRT phase. They have a  $P2_1/n$  symmetry with two molecules in the cell with the parameters  $a = 5.9301(9) \text{ \AA}$ ,  $b = 7.6045(1) \text{ \AA}$ ,  $c = 9.0316(1) \text{ \AA}$ ,  $\beta = 93.151(1)^\circ$ , and  $V = 406.67(1) \text{ \AA}^3$  under ambient conditions. The APRT  $\rightarrow$  HP phase transition takes place without changing the crystal symmetry at pressures higher than 3 GPa and room temperature. In a similar way, it was described earlier in ref.<sup>12</sup> where no significant changes of the diffraction pattern were observed after the phase transition at high pressure. Under slow cooling, the APRT phase transforms to the  $LT_1$  phase, which is triclinic and can be

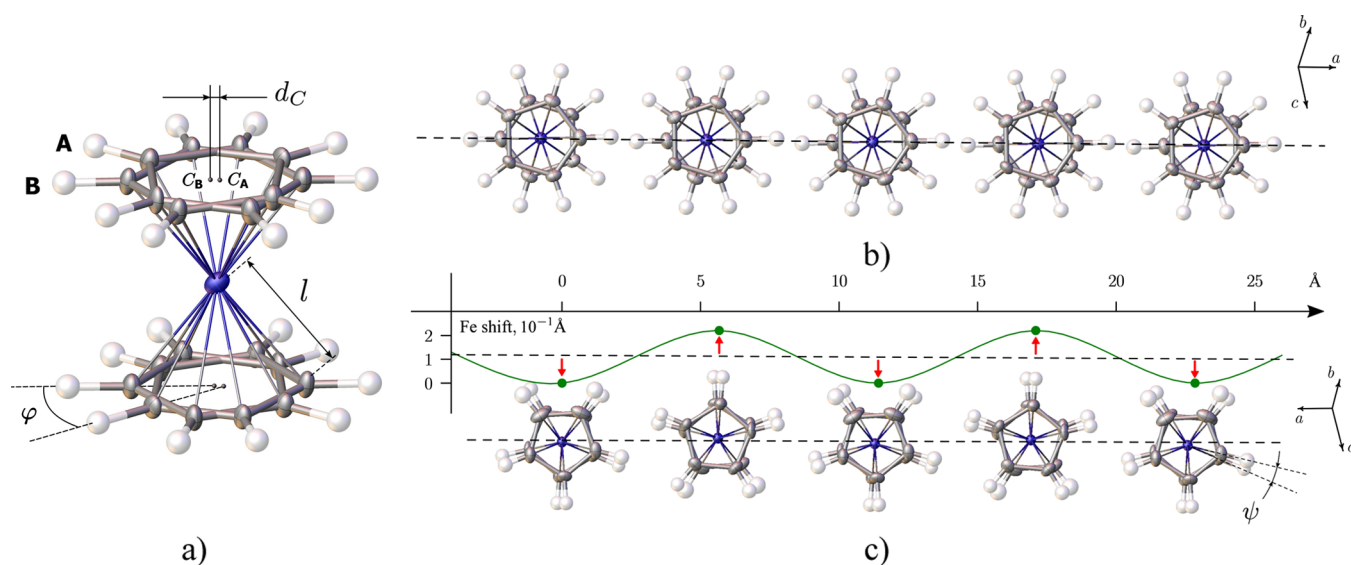


**Figure 1.** Basic parameters of a disordered  $\text{Fe}^{2+}\{\text{C}_5\text{H}_5\}_2^-$  molecular structure (a); ferrocene chain in the high-pressure phase HP (5.5 GPa) (b); and ferrocene chain in the low-temperature phase  $\text{LT}_1$  (105 K) (c).

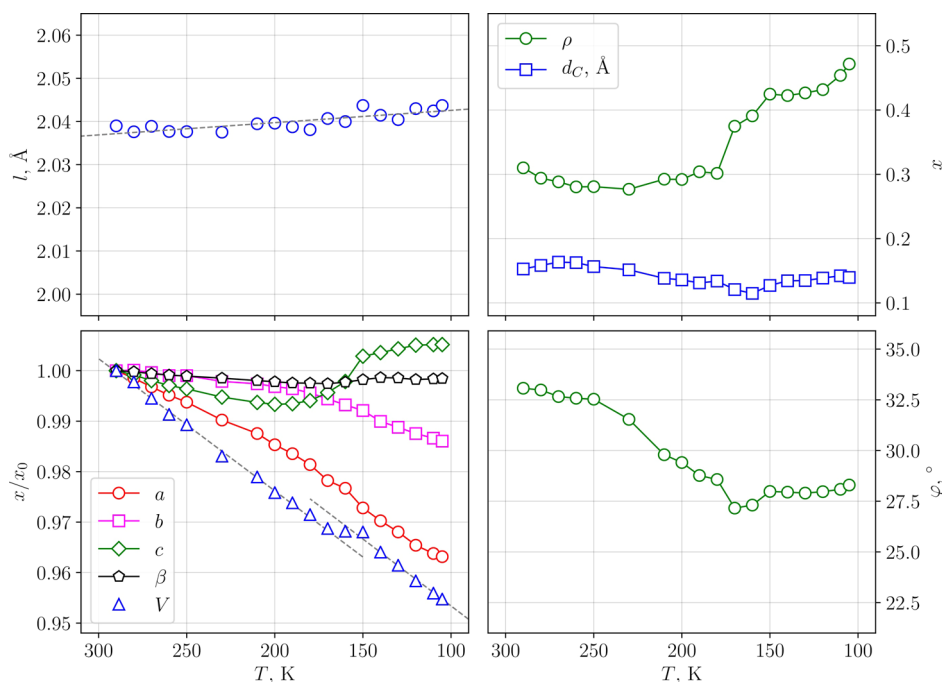


**Figure 2.** Evolution of the crystal structure and molecular conformation parameters in pristine ferrocene crystals during slow heating from 100 to 290 K.

solved in the  $P\bar{1}$  cell. At 105 K, the crystals have the unit cell parameters  $a = 9.0931(5) \text{ \AA}$ ,  $b = 9.4123(7) \text{ \AA}$ ,  $c = 9.4545(5) \text{ \AA}$ ,  $\alpha = 105.475(6)^\circ$ ,  $\beta = 91.660(4)^\circ$ ,  $\gamma = 91.982(5)^\circ$ , and  $V = 778.77(9) \text{ \AA}^3$  and are twinned (0.27:0.73) according to the law

$$\begin{pmatrix} -1 & 0 & 0 \\ 0 & 0 & 1 \\ 0 & -1 & 0 \end{pmatrix} \begin{pmatrix} h \\ k \\ l \end{pmatrix}_{\text{twin}_1} = \begin{pmatrix} h \\ k \\ l \end{pmatrix}_{\text{twin}_2}$$

Note also that it is possible to consider the low-temperature phase  $\text{LT}_1$  as a commensurate monoclinic  $P2_1/n$  phase with a smaller cell volume. Such representation allows the comparison of the crystallographic data of  $\text{LT}_1$  with those of APRT and HP crystal phases considering the same symmetry of their cells.

The main reason why it is preferable to use an equally symmetric cell is the possibility of using a slightly refined orientation matrix during low-temperature experiments instead of finding a new one at each new temperature.

Structural solutions were performed for all APRT,  $\text{LT}_1$ , and HP phases. An asymmetric unit of the monoclinic APRT phase contains half of a ferrocene molecule with disordered positions of Cp rings. These positions, denoted as A and B in Figure 1a, are rotated with respect to each other by the angle  $\varphi$ . Their gravity centers  $C_A$  and  $C_B$  are shifted relative to each other by the distance  $d_C$ , whereas the atomic position of Fe is symmetrically fixed at the center of the unit cell. The crystal structure of the HP phase is similar to that of the previous APRT phase except for Fc molecule orientations, which are

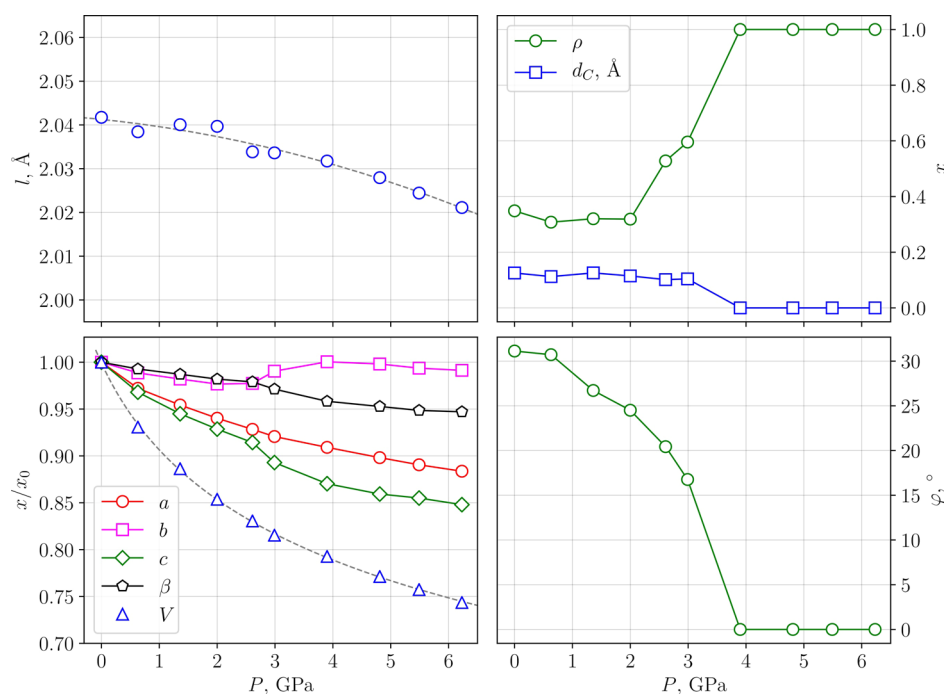


**Figure 3.** Evolution of the crystal structure and molecular conformation parameters in pristine ferrocene crystals at high pressure.

completely ordered because high pressure firmly stabilizes the staggered molecule conformation. The crystal structure of the monoclinic  $P2_1/n$  phase consists of ferrocene molecules packed into strictly linear chains, as shown in Figure 1b.

The crystals in the triclinic  $LT_1$  phase have a doubled unit cell (with respect to the monoclinic phase) with two unique halves of ferrocene molecules. All these ferrocene fragments have only one Cp ring; thus, the whole molecule is ordered. The angle  $\psi$  between two opposite Cp rings is  $8.2^\circ$  (see Figure 1c), which is close to the earlier observed value.<sup>6</sup> The main difference between  $P2_1/n$  and  $P\bar{1}$  structures is that Fc molecules in the triclinic  $LT_1$  phase are “frozen” in a near-eclipsed conformation. They form chains in a zigzag-shaped manner, where the maximum displacement of Fe atom positions from an average line is  $\pm 0.11$  Å. Considering the  $LT_1$  phase as the monoclinic one, its unit cell must be halved, and it becomes almost the same as the unit cell of the APRT phase, while the occupancies of the disordered Cp rings of a ferrocene molecule should be nearly equal.

**3.2. Molecular Conformations.** The graphs in Figure 2 show the parameters of the Fc crystal structure and molecular conformation at various temperatures. The Fe–C bond length  $l$  demonstrates weak temperature dependence (open circles), which fits well with the linear dependence  $l(T) = 2.045 - 2.84 \times 10^{-5} T$  (dotted line, the upper left panel in Figure 2). According to this equation, the average carbon–iron bond length takes the value 2.036 Å at room temperature. The upper right panel in Figure 2 demonstrates the distance between the centers of A and B positions of disordered Cp rings  $d_C$  (see Figure 1a) and their minor position occupancy  $\rho$  at different temperatures. The latter does not show substantial changes in the temperature range of 300–275 K ( $\rho \approx 0.29$ ) but rapidly increases, tending to  $\rho = 0.5$  when temperature decreases below 275 K. Thus, the occupancies of the Cp ring positions tend to be equal after the APRT  $\rightarrow$   $LT_1$  phase transition (monoclinic settings) and subsequent cooling. More precisely, according to the accurate crystallographic data,  $\rho$  is equal to

0.47 at  $T = 100$  K instead of 0.5; this discrepancy may relate to the crystal twinning with unequal domains, which accompanies the phase transition. In contrast to  $\rho$ , when temperature decreases, the  $d_C$  distance slightly oscillates around an average value of 0.141 Å, becoming practically constant in the  $LT_1$  phase. The relative cell volume  $V(T)/V_0$  (see Figure 2, lower left panel) shows linear temperature dependence through the temperature range under study with singularity near the APRT  $\rightarrow$   $LT_1$  phase transition. The slope of the  $V(T)$  curve slightly changes at the transition temperature due to a small increase in the thermal expansion coefficient  $\beta = 1/V(\partial V/\partial T)_P$  from  $\beta_{\text{APRT}} = 2.62 \times 10^{-4} \text{ K}^{-1}$  to  $\beta_{\text{LT}_1} = 2.74 \times 10^{-4} \text{ K}^{-1}$ , while the cell volume changes by  $\Delta V = 1.5 \text{ \AA}^3$ . The APRT  $\rightarrow$   $LT_1$  transition temperature defined from the peak position in the first-order derivative of the  $V(T)/V_0$  curve is 161.3 K. Thus, structural transition under slow heating occurs at a temperature that is very close to that obtained in calorimetry measurements.<sup>7</sup> A misorientation angle  $\varphi = 33.2^\circ$  under ambient conditions (see Figure 1a) gradually decreases with temperature and stabilizes at  $27.8^\circ$  at  $T < 163$  K. In the monoclinic  $LT_1$  phase, the  $\varphi$  angle means a rotation angle between two ferrocene molecules that are present in the triclinic cell of the  $LT_1$  phase.

Plots in Figure 3 show the evolution of unit cell parameters and molecular conformation in a pristine ferrocene crystal at high pressures up to 6 GPa. Unlike the APRT  $\rightarrow$   $LT_1$  phase transition, the dependence of volume on pressure looks smooth and does not show any peculiarities within the accuracy of measurements in the pressure range where the APRT  $\rightarrow$  HP transformation is expected. Fitting of the experimental data using the Murnaghan equation of state  $V/V_0 = (1 + P \times (B'_0/B_0))^{-1/B'_0}$  gives the value of the bulk modulus of  $B(P) = B_0 + B'_0 P$ , where  $B_0 = 7.49$  GPa and  $B'_0 = 6.17$ . A rather broad transition region from the disordered APRT phase to the ordered HP phase is located between 3 and 4 GPa. During the phase transition, decreasing pressure dependence of the

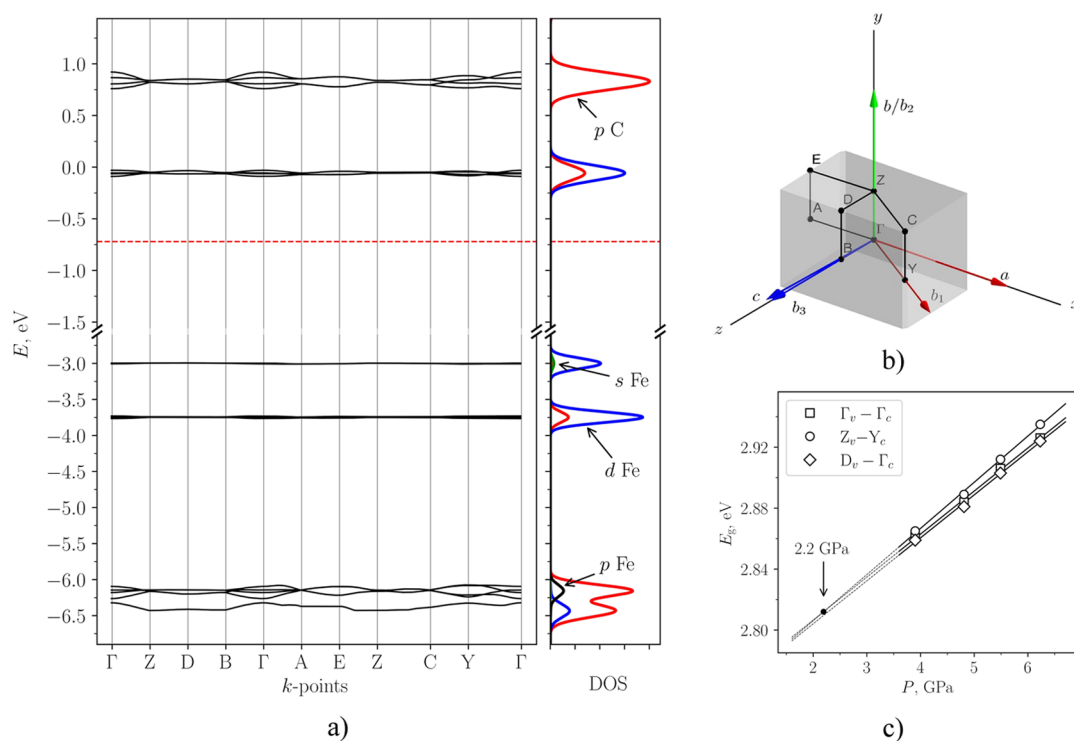


**Figure 4.** Band structure and Fermi smeared density of states of the HP phase at 5.5 GPa (a); first Brillouin zone and  $a$ ,  $b$ , and  $c$  directions are given for a monoclinic unit cell in the standard setting with  $\beta > 90^\circ$ , where  $b_i$  marks reciprocal space vectors for a primitive unit cell (b); and pressure dependence of the fundamental gap energy  $E_g$  (c).

lattice parameter  $a(P)$  and unit cell volume  $V(P)$  is smooth, whereas  $b(P)$ ,  $c(P)$ , and  $\beta(P)$  lattice parameters show significant multidirectional changes up to 2–5%. The transition begins at a pressure of  $\sim 3$  GPa, as found from the singularity in the first derivative of the most volatile  $b$  parameter. At this particular pressure,  $\beta = 90^\circ$  so that at the moment of a pressure-induced transition, a ferrocene crystal can be treated as “orthorhombic” with higher symmetry. Between 3 and 4 GPa, the  $b$ -axis parameter increases with pressure, whereas the  $c$ -axis parameter decreases, while after 4 GPa the  $b(P)$  and  $c(P)$  curves approach asymptotic dependence ( $8.028 - 0.071 \cdot P$ ). The average  $b$  and  $c$  parameter values are  $\sim 7.6$  Å at the highest pressure of 6.23 GPa, whereas their difference is  $\sim 0.12$  Å. According to the structural analysis, the Fe–C bond length  $l$  decreases with pressure as  $l = 2.043 - 1.36 \times 10^{-3} \cdot P - 3.04 \times 10^{-4} \cdot P^2$ , where  $P$  is the pressure given in gigapascal. The value of  $l$  under ambient conditions defined in X-ray experiments at high pressure and those at low temperatures slightly differ. Most likely, this is related to the somewhat less accuracy of X-ray measurements at high pressure due to the limitations of the design of the DAC. The distance between centroids of two Cp rings  $d_C = 0.116$  Å also remains almost unchanged up to 3 GPa; however, at higher pressure, after the APRT  $\rightarrow$  HP phase transition, the molecules become completely ordered so that  $\rho = 0$ ,  $d_C = 0$ , and  $\varphi = 0$  (i.e., all Fc are in the staggered conformation) for pressures higher than 4 GPa.

**3.3. Electronic Structure Calculations.** Calculation of an electronic band structure in the APRT phase is a difficult task due to the structural disorder of Cp rings. Thus, the calculations were performed for the monoclinic HP and triclinic  $LT_1$  crystal phases using *DFTB+* software and the obtained X-ray structural data. The panels in Figure 4

represent the electronic band structure of the ordered HP phase of a Fc crystal and variation of the fundamental gap energy  $E_g$  at  $P > 3$  GPa. The band structure of the  $LT_1$  phase is similar to that of the HP phase with the only difference being the fact that most of the bands are doubly split. The splitting is rather small; for instance, it is  $\sim 20$  meV for a narrow valence band and  $\sim 50$  meV for a conduction band. The splitting is associated with the presence of two symmetrically non-equivalent Fc molecules in their actually triclinic structure. As seen from the density of states in Figure 4, the narrow valence and conduction bands are formed by the p orbitals of a carbon atom and by the d orbitals and, to a small extent, the s orbitals of an iron atom. These bands are the result of the interaction of the highest occupied molecular orbital (HOMO) and lowest unoccupied molecular orbital (LUMO) levels of the ferrocene molecule. The accurate B3LYP calculation of a single Fc molecule and subsequent contribution analysis based on the Mulliken scheme of population give the main components of  $e_{2g}$  HOMO (86% of iron mostly  $d_{x^2-y^2}$  and  $d_{xy}$ ) and  $e_{1g}$  LUMO (58% of iron  $d_{xz}$  and  $d_{yz}$  orbitals and 38% of carbon  $p_z$  sub-shells), which is close to the *DFTB+* results. The plot in Figure 4c demonstrates the pressure dependence of the optical gap  $E_g(P)$  between symmetry points  $\Gamma$ – $\Gamma$  (direct transition),  $Z$ – $Y$ , and  $D$ – $\Gamma$  (indirect transitions), which might be expressed as  $E_g(P) = E_0 + b \cdot P$ , where  $E_0$  is the initial gap value and  $b = \partial E_g / \partial P$  is the pressure coefficient. The magnitude of the pressure coefficients  $b$  and the gap value  $E_0$  for these three transitions are very close to each other (they are shown in Table 1). The extension of pressure dependence for direct  $\Gamma$ – $\Gamma$  and indirect  $Z$ – $Y$  transitions out of the HP phase region shows their crossing at  $\sim 2$  GPa.

The quantitative measurements of the gap value using optical absorption spectroscopy are quite a difficult task

**Table 1. Calculated Initial Band Gap  $E_0$  and Coefficients of the Linear Pressure Shift  $\Delta E_g(P)$  in the HP Phase of Ferrocene Crystals**

directions	$E_0$ (eV)	$b$ , (eV/GPa)
$\Gamma_v-\Gamma_c$	2.750	0.028
$Z_v-Y_c$	2.746	0.030
$D_v-\Gamma_c$	2.748	0.028

because it requires very thin uniform flat crystals. Nevertheless, the pressure shift of the energy gap  $E_g(P)$  can be determined from the optical transmission spectra at high pressure when comparing spectral positions with the same transmittance at different pressures (Figure 5, left panel). To improve the accuracy of measurements, the optical transmission spectra were measured in the same place on the sample during a gradual increase in the pressure. The data were plotted for two different transmittances shown by squares and circles in the right panel of Figure 5. Smooth dependence of  $\Delta E_g(P)$  on pressure shows a jump of about 14.5 meV at  $P = 2$  GPa; however, it is well-fitted by linear dependence with slopes of  $12.6 \pm 1.3$  meV GPa<sup>-1</sup> (before the singularity) and  $12.1 \pm 1.1$  meV GPa<sup>-1</sup> (after the singularity) (open and filled symbols, respectively). These values are more than 2 times smaller than the calculated pressure coefficient of 28 meV GPa<sup>-1</sup> obtained in the DFTB+ calculations of the pressure-induced energy gap shift in the  $\Gamma$ -point of the Brillion zone (see Table 1).

**3.4. Phonon Spectral Analysis.** The calculated Raman spectrum of the staggered molecular conformation contains two intense bands: the lower energy band with  $\nu_{br} = 288.56$  cm<sup>-1</sup> corresponds to the Fe–Cp breathing mode and doubly degenerate  $\nu_{sh} = 364.17$  cm<sup>-1</sup> corresponds to the molecular shear mode. For the eclipsed conformation, both bands are shifted to lower energies by  $\Delta\nu_{br} = -2.65$  cm<sup>-1</sup> and  $\Delta\nu_{sh} = -9.45$  cm<sup>-1</sup>. The frequencies of these modes in the Raman spectra under ambient conditions are  $\sim 29$  cm<sup>-1</sup> larger than the calculated values of  $\nu_{br}$  and  $\nu_{sh}$ ; therefore, the latter are underestimated. In addition, they are almost split, showing weak shoulders near an intense central peak. The split components are related to  $D_{5h}$  and  $D_{5d}$  molecular conformations, while their splitting of  $\sim 6$  cm<sup>-1</sup> is between the

calculated magnitudes of  $\Delta\nu_{br}$  and  $\Delta\nu_{sh}$  for eclipsed and staggered conformations. Surprisingly, both split components in Raman spectra of the APRT phase appear in the HP phase that should contain only the  $D_{5d}$  staggered conformation. This phenomenon is not completely understood and requires further study. At the moment, we suppose that it may be related to the influence of the sample surface in back-scattering Raman measurements. Note that the breathing and shear modes correspond to the lowest intramolecular phonons. Thus, the phonon bands with smaller frequencies in the Raman spectra of a ferrocene crystal should be attributed to intermolecular phonons. The broad band of an intermolecular phonon at the beginning of the Raman spectrum can be successfully resolved at pressures higher than 1 GPa. Under ambient conditions, this mode cannot be observed since an appropriate energy region is very close to the edge filter cutoff. When pressure increases, the broad band shifts to higher energy and forms five narrow bands near APRT  $\rightarrow$  HP phase transition.

Figure 6 depicts the Raman spectra of a Fc single crystal in the energy region of 75–560 cm<sup>-1</sup> at pressures up to 10.5 GPa (left panel), pressure dependence of inter- and intramolecular phonon modes (central panel), and pressure dependence of the full width at the half maximum (FWHM) for some Raman bands (right panel). The lower spectrum in the left panel is the calculated Raman spectrum of an isolated ferrocene molecule, while in the above panel, the experimental Raman spectra of a ferrocene crystal at ambient and high pressure are depicted. Numerical calculations were performed using the B3LYP method for two ferrocene conformations—eclipsed ( $D_{5h}$  symmetry) and staggered ( $D_{5d}$  symmetry). According to the earlier publication,<sup>5</sup> these conformations are very close in energy, while a small energy barrier of at least  $\sim 21$  meV separates them.<sup>5</sup> More precisely, our B3LYP calculations of the total energy of a  $D_{5h}$  ferrocene molecule show that it is 14 meV lower than that of a molecule with a  $D_{5d}$  symmetry. In a pristine ferrocene crystal, both conformations coexist, and their relative populations depend on the crystal field,<sup>3,12,13</sup> while the eclipsed conformation is widespread in various ferrocene complexes and has been studied extensively.<sup>14,15</sup>

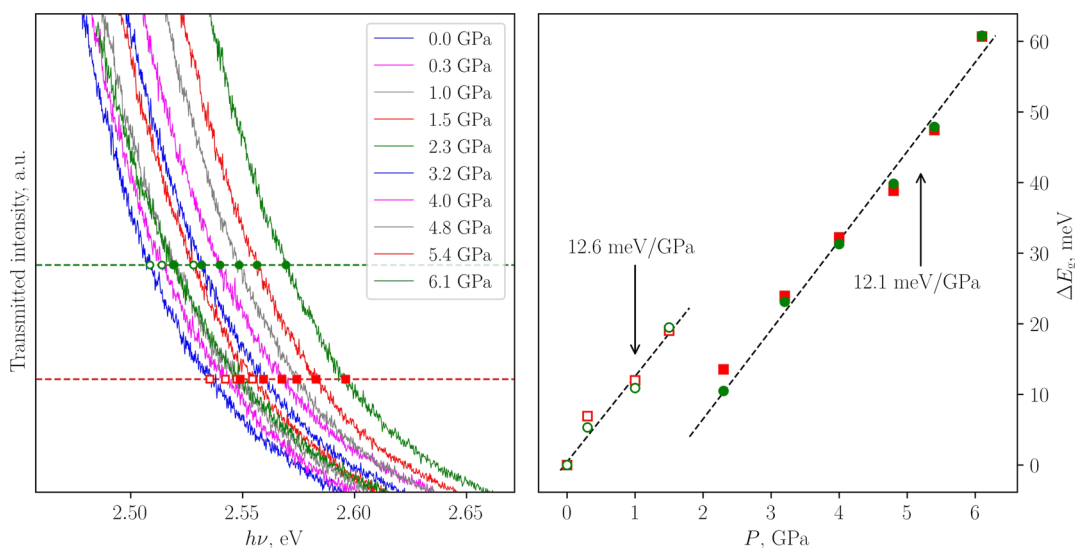


**Figure 5.** Optical transmission spectra of Fc crystals at high pressure (left panel) and  $\Delta E_g(P)$  dependence.

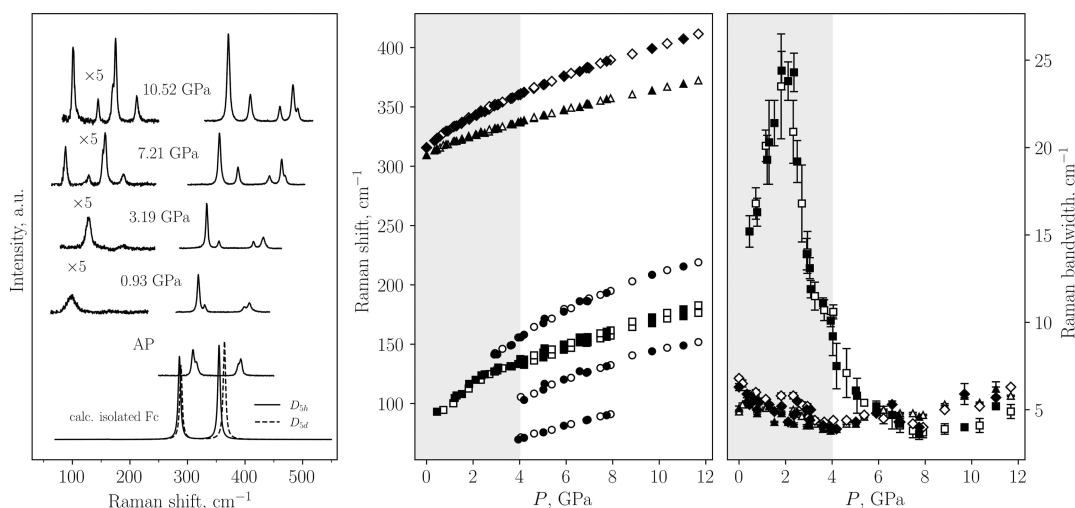


**Figure 6.** Raman spectra of Fc crystals at high pressure and pressure behavior of phonon modes. Open symbols—increase of pressure and solid symbols—decrease of pressure.

The central panel in Figure 6 shows the pressure dependence of two split components of the intramolecular breathing mode and the intermolecular phonon modes. Open and solid symbols correspond to pressure increase and decrease cycles, respectively, while the data were obtained in three independent pressure runs. All data match well within the accuracy of measurements, showing the reversibility and reproducibility of measurements at high pressure. The splitting of the  $\nu_{br}$  intramolecular mode reasonably increases with pressure, while at  $P \geq 1.8$  GPa, it increases much more due to the difference in the pressure coefficients of split components. The intermolecular phonon modes show an intriguing pressure behavior. The Raman spectrum at low pressure contains one broad band, which shifts rapidly with pressure; the pressure shift is well-fitted by the linear dependence  $\omega = 87.4 \text{ cm}^{-1} + 14.0 \text{ cm}^{-1}/\text{GPa} P$  at pressures up to 3 GPa. At higher pressure, this band splits, forming five narrow components near 4 GPa. The pressure shift of new bands is linear at pressures up to  $\sim 6$  GPa, while it becomes sublinear at a subsequent increase in the pressure, which is typical for molecular crystals.<sup>26</sup> The pressure coefficients of the split bands in the linear region are smaller than those of the broad band and vary between 6.4 and  $12.4 \text{ cm}^{-1}/\text{GPa}$ . More precisely, the pressure shift of these modes may be fitted by the second-order equation  $\omega = a + bP + cP^2$ , where the linear pressure coefficient  $b = \partial\nu/\partial P$  varies in the abovementioned range.

The right panel in Figure 6 shows the pressure dependence of FWHM for two split components of the intramolecular breathing mode  $\nu_{br}$  and the broad intermolecular phonon mode of a ferrocene crystal. Data for different modes are shown by the same symbols as those in the central panel of Figure 6. The FWHM of the split breathing mode is considerably smaller than that of the intermolecular mode and decreases from  $\sim 7 \text{ cm}^{-1}$  at ambient pressure to  $\sim 4 \text{ cm}^{-1}$  at 4 GPa. In contrast, the FWHM of the intermolecular phonon mode increases with pressure from  $\sim 15 \text{ cm}^{-1}$  at low pressure to the maximum of  $\sim 25 \text{ cm}^{-1}$  near 2 GPa and then decreases to  $\sim 8 \text{ cm}^{-1}$  at 4 GPa. In our opinion, a very broad intermolecular phonon band and unusual pressure behavior of FWHM are related to the orientation disorder of ferrocene molecules in the APRT phase. Generally, narrow peaks in the first-order Raman spectra of crystalline solids are due to the

impulse selection rules, which allow Raman scattering for phonons in the  $\Gamma$ -point of the Brillouin zone.<sup>27</sup> In the case of structural/orientation disorder, the impulse selection rules are violated, and the intermolecular phonon bands show the phonon density of states.<sup>28</sup> Thus, fast jumps of a Fc molecule between  $D_{Sh}$  and  $D_{Sd}$  conformations lead to a decrease in the intermolecular phonon lifetime and broadening of bands.<sup>29</sup> We suppose that the rate of jumps varies because of changes in a crystal field caused by pressure; it reaches the maximum at 2 GPa while decreasing to zero at 4 GPa after the ordering of molecules in the staggered conformation. In other words, the small lifetime of the molecular conformation restricts the lifetime of intermolecular phonons, resulting in the broadening of bands in Raman spectra.

#### 4. CONCLUSIONS

The X-ray diffraction studies of pristine  $\text{Fe}^{2+}(\eta^5\text{-C}_5\text{H}_5)_2^-$  crystals at high pressure and low temperature have shown that intramolecular disordering parameters, associated with two possible occupations of Cp rings of a ferrocene molecule and the angle between them, vary with temperature and pressure, resulting in complete ordering of ferrocene molecules in low-temperature ( $\leq 161.3$  K) and high-pressure ( $\geq 3$  GPa) phases. The accurate structural analysis has provided quantitative data on the internal molecular properties: the length of the Fe–C bond, the disorder of the positions of a Cp ring and its rotation angle, and unit cell parameter variation with pressure and temperature during the APRT  $\rightarrow$  LT<sub>1</sub> and APRT  $\rightarrow$  HP phase transitions. The latter shows structural changes starting out at 3 GPa and manifests significant changes in the Raman spectra. They are related to the splitting of a broad intermolecular phonon band to five sharp peaks when the molecules are ordered in the staggered conformation at the last stage of the APRT  $\rightarrow$  HP phase transition at 4 GPa. Fast jumps of a Fc molecule between  $D_{Sh}$  and  $D_{Sd}$  conformations lead to a decrease in the phonon lifetime and broadening of phonon bands. The rate of jumps increases to the maximum at 2 GPa and then decreases to zero at 4 GPa when the transition to HP is completed. Numerical calculations of the electronic band structure in the HP phase at various pressures show that the direct energy gap  $E_g$  in the center of the Brillouin zone linearly increases with pressure with the coefficient of 28 meV

GPa<sup>-1</sup>. Optical transmission measurements at high pressure show an abrupt decrease in the fundamental gap by ~14.5 meV near 2 GPa, while pressure dependence is linear with slopes of  $12.6 \pm 1.3$  meV GPa<sup>-1</sup> (before the singularity) and  $12.1 \pm 1.1$  meV GPa<sup>-1</sup> (after the singularity). The magnitude of the fundamental gap jump of 14.5 meV is close to the energy of intermolecular phonon modes and may be related to a crossover of indirect and direct optical transitions near 2 GPa.

## AUTHOR INFORMATION

### Corresponding Author

Alexey V. Kuzmin – Institute of Solid State Physics RAS,  
Chernogolovka, Moscow Region 142432, Russia;  
orcid.org/0000-0001-8218-4058; Email: kuzminav@  
issp.ac.ru

### Authors

Konstantin P. Meletov – Institute of Solid State Physics RAS,  
Chernogolovka, Moscow Region 142432, Russia  
Maxim A. Faraonov – Institute of Problems of Chemical  
Physics RAS, Chernogolovka, Moscow Region 142432,  
Russia; orcid.org/0000-0003-0805-601X

Complete contact information is available at:  
<https://pubs.acs.org/10.1021/acs.jpcc.1c10063>

### Notes

The authors declare no competing financial interest.

## ACKNOWLEDGMENTS

Structural analysis and spectroscopic characterization of ferrocene crystals were carried out within the research project of ISSP RAS funded by the Ministry of Science and Higher Education of the Russian Federation (registration number AAAA-A17-117121120049-3). All single crystals were obtained with the support of the Ministry of Science and Higher Education of the Russian Federation (registration number AAAA-A19-119092390079-8).

## REFERENCES

- (1) Kealy, T. J.; Pauson, P. L. A new type of organo-iron compound. *Nature* **1951**, *168*, 1039–1040 Springer Science and Business Media {LLC}.
- (2) Miller, S. A.; Tebboth, J. A.; Tremaine, J. F. Dicyclopentadienyliron. *J. Chem. Soc.* **1952**, *632*, 632–635.
- (3) Haaland, A.; Nilsson, J.-E. The determination of the barrier to internal rotation in ferrocene and ruthenocene by means of electron diffraction. *Chem. Commun.* **1968**, *2*, 88–89.
- (4) Xu, Z.-F.; Xie, Y.; Feng, W.-L.; Schaefer, H. F. Systematic investigation of electronic and molecular structures for the first transition metal series metallocenes  $M(C_5H_5)_2$  ( $M = V, Cr, Mn, Fe, Co, Ni$ ). *J. Phys. Chem. A* **2003**, *107*, 2716–2729.
- (5) Mohammadi, N.; Ganesan, A.; Chantler, C. T.; Wang, F. Differentiation of ferrocene  $D_{3d}$  and  $D_{5h}$  conformers using IR spectroscopy. *J. Organomet. Chem.* **2012**, *713*, 51–59.
- (6) Seiler, P.; Dunitz, J. D. The structure of triclinic ferrocene at 101, 123 and 148 K. *Acta Crystallogr., Sect. B: Struct. Crystallogr. Cryst. Chem.* **1979**, *35*, 2020–2032.
- (7) Edwards, J. W.; Kington, G. L.; Mason, R. The thermodynamic properties of ferrocene. Part 1. The low-temperature transition in ferrocene crystals. *Trans. Faraday Soc.* **1960**, *56*, 660–667.
- (8) Ogasahara, K.; Sorai, M.; Suga, H. New finding of a stable low-temperature phase in ferrocene crystal. *Chem. Phys. Lett.* **1979**, *68*, 457–460.
- (9) Seiler, P.; Dunitz, J. D. Low-temperature crystallization of orthorhombic ferrocene: structure analysis at 98 K. *Acta Crystallogr., Sect. B: Struct. Crystallogr. Cryst. Chem.* **1982**, *38*, 1741–1745.
- (10) Duecker, H. C.; Lippincott, E. R. Phase transformation in ferrocene. *J. Chem. Phys.* **1967**, *46*, 3691–3692.
- (11) Zhorin, V. A.; Maksimych, A. V.; Ponomarenko, A. T.; Enikolopyan, N. S. Electrophysical characteristics of several organic compounds at high pressures and high pressures combined with shearing strains. *Bull. Acad. Sci. USSR, Div. Chem. Sci.* **1979**, *28*, 2078–2082.
- (12) Paliwoda, D.; Kowalska, K.; Hanfland, M.; Katrusiak, A. U-turn compression to a new isostructural ferrocene phase. *J. Phys. Chem. Lett.* **2013**, *4*, 4032–4037.
- (13) Coriani, S.; Haaland, A.; Helgaker, T.; Jørgensen, P. The equilibrium structure of ferrocene. *ChemPhysChem* **2006**, *7*, 245–249.
- (14) Kuzmin, A. V.; Khasanov, S. S.; Meletov, K. P.; Konarev, D. V. High-pressure behavior of the crystal structure of the fullerene molecular complex with ferrocene  $C_{60}\{Fe(C_5H_5)_2\}_2$ . Fullerenes, Nanotubes. *Carbon Nanostruct.* **2020**, *28*, 295–298.
- (15) Kuzmin, A. V.; Meletov, K. P.; Khasanov, S. S.; Faraonov, M. A. Pressure-induced donor-acceptor charge transfer in a fullerene molecular complex with ferrocene. *J. Phys. Chem. C* **2021**, *125*, 16576–16582.
- (16) *CrysAlisPro*, 1.171.40.67a; Rigaku Oxford Diffraction, 2019.
- (17) Dolomanov, O. V.; Bourhis, L. J.; Gildea, R. J.; et al. OLEX2: A complete structure solution, refinement and analysis program. *J. Appl. Crystallogr.* **2009**, *42*, 339–341.
- (18) Sheldrick, G. M. SHELXL-2018/3, Program for the Solution and Refining of Crystal Structures; University of Göttingen: Göttingen, Germany, 2018.
- (19) Sheldrick, G. M. SHELXT - Integrated space-group and crystal-structure determination. *Acta Crystallogr., Sect. A: Found. Adv.* **2015**, *71*, 3–8.
- (20) Aradi, B.; Hourahine, B.; Frauenheim, T. DFTB+ a sparse matrix-based implementation of the DFTB method. *J. Phys. Chem. A* **2007**, *111*, 5678–5684.
- (21) Elstner, M.; Porezag, D.; Jungnickel, G.; et al. Self-consistent-charge density-functional tight-binding method for simulations of complex materials properties. *Phys. Rev. B: Condens. Matter Mater. Phys.* **1998**, *58*, 7260–7268.
- (22) Zheng, G.; Witek, H. A.; Bobadova-Parvanova, P.; et al. Parameter calibration of transition-metal elements for the spin-polarized self-consistent-charge density-functional tight-binding (DFTB) Method: Sc, Ti, Fe, Co, and Ni. *J. Chem. Theory Comput.* **2007**, *3*, 1349–1367.
- (23) Becke, A. D. Density-functional thermochemistry. III. The role of exact exchange. *J. Chem. Phys.* **1993**, *98*, 5648–5652.
- (24) Lee, C.; Yang, W.; Parr, R. G. Development of the Colle-Salvetti correlation-energy formula into a functional of the electron density. *Phys. Rev. B: Condens. Matter Mater. Phys.* **1988**, *37*, 785–789.
- (25) Granovsky, A. A. Firefly, version 8 [Electronic resource]. URL: <http://classic.chem.msu.su/gran/firefly/index.html>.
- (26) Meletov, K. P. Phonon spectrum of a naphthalene crystal at a high pressure: Influence of shortened distances on the lattice and intramolecular vibrations. *Phys. Solid State* **2013**, *55*, 581–588.
- (27) Duckett, S.; Yarwood, J.; Douthwaite, R. *Spectroscopic Properties of Inorganic and Organometallic Compounds: Techniques, Materials and Applications*; Royal Society of Chemistry, 2012; Vol. 43.
- (28) Kardona, M. *Light Scattering in Solids*; Springer-Verlag, 1975; pp 237–242.
- (29) Fuchs, H. D.; Grein, C. H.; Devlen, R. I.; Kuhl, J.; Cardona, M. Anharmonic decay time, isotopic scattering time, and inhomogeneous line broadening of optical phonons in <sup>70</sup>Ge, <sup>76</sup>Ge, and natural Ge crystals. *Phys. Rev. B: Condens. Matter Mater. Phys.* **1991**, *44*, 8633–8642.